African Journal of Advanced Pure and Applied Sciences (AJAPAS)
Online ISSN: 2957-644X
Volume 4, Issue 3, 2025
Page No: 38-54
Website: https://aaasjournals.com/index.php/ajapas/index
ISI 2025: 1.126 **SJIFactor 2024: 6.752** **معامل التأثير العربي: 1.62**

Natural Convection in Closed-Sided Inclined Channels

Ahmed Habeb *
Faculty of Science, Aljufra University, Houn, Libya

الحمل الحراري الحر في القنوات المائلة ذات الجوانب المغلقة

أحمد حبيب *
كلية العلوم، جامعة الجفرة، هون، ليبيا

*Corresponding author: ahmed.habeb@ju.edu.ly

Received: May 11, 2025	Accepted: July 02, 2025	Published: July 12, 2025

Abstract:
Airflow characteristics due to natural convection heat transfer along an inclined channel have been experimentally studied in the current work. The main object of the study was to investigate the airflow and heat transfer under the variations of uniform of heat flux, aspect ratio and the inclination angle. Four values of heat inputs (5 W, 10 W, 15 W, and 20 W), three different aspect ratios (0.45, 0.55 and 0.65) and three various inclination angles (30°, 45°, and 60°) were all tested on channel measured 0.1m by 0.1m. Extensive analysis was performed resulting to practical outcomes. It was found that mass flow rate increases as the heat input and channel depth (or aspect ratio) increase, but decreases as the inclination angle increases. In addition, the average heat-transfer coefficient increases as the heat input increases, but decreases as the channel depth (or aspect ratio) and inclination angle increase. Dimensionless correlations of two and three independent variables were derived for the Nusselt and Reynolds numbers as a function of modified Rayleigh numbers, aspect ratios and inclination angles.

Keywords: Natural Convection, Airflow, Inclined Channels.

الملخص:
في العمل الحالي، تمت دراسة خصائص تدفق الهواء الناتجة عن انتقال الحرارة بالحمل الحراري الطبيعي على طول قناة مائلة معملياً. كان الهدف الرئيسي من البحث هو دراسة تدفق الهواء وانتقال الحرارة في ظل متغيرات التدفق الحراري المنتظم ونسبة العمق إلى الارتفاع وزاوية الميل. تم اختبار أربع قيم لمدخلات الحرارة (5 W, 20 W, 15 W, 10 W) وثلاث نسب عمق إلى ارتفاع مختلفة (0.45, 0.55, 0.65) وثلاث زوايا ميل مختلفة (30°, 45° , 60°) على قناة مقاسها 0.1 متر × 0.1 متر. تم إجراء تحليل مكثف أدى إلى استنتاج نتائج عملية. وجد أن معدل التدفق الكتلي يزداد مع زيادة كمية الحرارة المضافة وعمق القناة (أو نسبة العمق إلى الارتفاع)، ولكنه ينخفض مع زيادة زاوية الميل. بالإضافة إلى ذلك، يزداد متوسط معامل انتقال الحرارة مع زيادة كمية الحرارة المضافة، ولكنه ينخفض مع زيادة عمق القناة (أو نسبة العمق إلى الارتفاع) وزاوية الميل. تم اشتقاق معادلات لابعدية لمتغيرين مستقلين وثلاثة متغيرات مستقلة لأرقام نسلت ورينولدز كدالة لرقم رايلي المعدل ونسب العمق إلى الارتفاع وزاوية الميل.

الكلمات المفتاحية: الحمل الحراري الطبيعي، تدفق الهواء، القنوات المائلة.

1. Introduction:

Natural convection heat transfer exists in many industrial applications, which encourages engineers and scientists to pay serious attention to performing theoretical and practical investigations. These studies cover a wide range of scientific applications and various physical aspects. Natural convection mechanism occurs as a result of the buoyancy forces due to temperature differences within the fluids (gas or liquid). In such applications, the heating source is introduced in two configurations: Uniform Wall Temperature (UWT) or Uniform Heat Flux (UHF). The

surface temperature of the former is known while the latter heat flux added to the surface is known. A considerable amount of foundational research has progressed steadily since the early 20th century, evolving from basic analytical models to complex numerical and experimental investigations that account, for example, the nature of the flow regime, asymmetry, and geometric configuration. This encompasses studies of buoyancy-driven flow along vertical and inclined surfaces/channels under either the UWT or UHF heating modes.

Natural convection airflow along a single vertical plate is a typical example applicable in electrical applications and heating systems, such as at radiator surfaces. The followings are some of the key studies concerned with thermal and hydrodynamic boundary layers developing along a single heated plate. Under UWT heating mode, [1, 2] studied experimental laminar, transition, and turbulent flow regimes and the thickness of the thermal boundary layer along a vertical heated flat plate. Laminar and turbulent boundary layer free convection from a vertical plate with uniform surface heat flux (UHF) was studied and numerical solution to the differential equations for heat transfer was obtained [3, 4]. In addition, [5] derived fundamental empirical equations for both laminar and turbulent free convection airflow from a vertical plate under the UHF and UWT heating mode. The outcomes of the early pioneering work of [6], who published an important study of natural convection from isothermal parallel plates, including both experimental data and theoretical treatments, provided significant information about heat dissipation from two parallel plates. He tested several sizes of heated plates at uniform temperatures and at various distances apart. Following this work, a sequence of related investigations was published on natural convection between heated surfaces under UWT configuration. The works of [7-13] reported experimental and numerical results on natural convection laminar flow between two parallel square plates and studied the effect of optimum spacing between the plates for UWT and UHF heating modes applicable for electronic cooling components. They also derived several empirical equations based on the system geometry and physical properties of the working fluid itself. Whilst most of the previous studies were concerned with laminar flow, [14, 15] investigated turbulent natural convection heat transfer in vertical channels. They developed an analysis to predict induced flow and heat transfer in an asymmetrically heated channel for the UWT case. The effect of radiation heat transfer on gases between parallel vertical plates was studies by applying three D CFD models [16] and temperature profiles and velocity profiles were obtained. In addition, Natural convection between the back of a vertical photovoltaic panel (heated surface) and fiber wall (insulated surface) was investigated experimentally and numerically [17]. Reference [18, 19] carried out indoor experimental studies of the airflow along a vertical channel (duct) simulating a passive solar air heater. They tested a wide range of aspect ratios (s/H) and heat inputs to examine their effect on the behavior of the airflow. Dimensionless correlations for the heat transfer coefficient and mass flow rate were derived. Inclined channel configurations can also be encountered in many applications, such as air and water solar collectors. Experimental investigation was performed by [20] on water as a working fluid under the UWT heating mode to study the effect of different s/H and inclination angle (2) on the fluid inside an inclined channel. The study verified the effect of the inclination angle on the heat transfer rate in the system and confirmed that the correlations are valid for inclined surfaces up to 45°. Following this study and under the UWT mode, [21-23] carried out experimental and numerical work on airflow inside an inclined channel. Variations of s/H, 2 and temperature variations of the heat surfaces were considered. Their extensive studies led to derived correlations for all cases. Finally, [24, 25] presented a numerical study of natural driven-convection flow within a tilted asymmetrically heated channel subjected to a constant heat flux was obtained. The effect of the channel inclination on thermal and flow behavior were shown through local Nusselt numbers, streamlines, isotherms, and axial velocity profiles.

The current work has been designed to evaluate the characteristics of natural convection airflow throughout an inclined channel, adjustable to three different angles (30°, 45°, and 60° relative to vertical axis). Most studies and outcome correlations have been based on the ordinary Grashof number, which is given by ($Gr(s) = g\,\beta\,\Delta T\,s^3/\nu^2$) where the temperatures are known. Thus, the uniqueness of this work lies in the fact that the airflow characterization is based on the UHF heating mode, and the outcome results, including empirical correlations, will cover different values of heat inputs, inclination angles and aspect ratios. The solution of the governing equations led to the introduction of several heat transfer parameters. Reference [26] derived for the first time the modified Grashof Number (Gr*) which was applicable to the uniform heat flux problems. The airflow under the UHF heating mode is based on convective heat transfer. Thus, defining the modified Grashof number is based on convective heat transfer and can be written as:

UHF heating mode Configuration: $$Gr^* = Gr(H)Nu(H) \Rightarrow Ra^* = Gr^*.Pr = \frac{g\,\beta\,q_c\,H^4}{\upsilon^2} \qquad (1)$$

The experimental studies and empirical correlations that were carried out under the UHF heating mode are unexpectedly few. For example, the early two works that dealt with UHF heating mode and derived correlations [27, 28]. The former [27] derived two correlations for a dimensionless heat transfer coefficient for laminar and

turbulent flow along surfaces. Whereas, the latter [28] derived theoretically correlations under the UHF heating mode for a fully developed flow between two vertical heated surfaces. The correlations of both studies were a function of the modified Rayleigh (Ra^*) number and other variables, but not suitable for small ducts. However, lately and on similar of the current test-rig [29], experimental work was carried out to investigate the performance of airflow on a vertical channel (θ=0°, with respect to vertical position). Several correlations regarding airflow and heat transfer rate were derived.

2. Experimental Apparatus and Procedure:

The experimental apparatus, devices and the main steps of experimental procedure used in the current project have been partially utilized by [29, 30], author of the present work. The experimental setup, as show in **Figure** 1, consists of a custom-designed vertical rectangular channel open at both the top and bottom ends while enclosed on the both sides. The channel dimensions were 10 cm in height (H) and 10 cm in width (w), forming an effective heating surface of a 0.01 m² area. The channel depth was an adjustable parameter and could be set between 45 mm, 55 mm and 65 mm (aspect ratio: s/H= 0.45, 0.55 and 0.65). The heating plate forming one of the channel walls was designed to provide the system with a desired power using an electrical resistance heater and facing upward. The heating element operated at four discrete power levels - 5 W, 10 W, 15 W, and 20 W - to simulate different uniform heat flux (UHF). Directly opposite and parallel the heated plate, a 2 mm thick aluminium sheet served as the unheated plate. The aluminium plate is externally insulated by a 10 mm layer of Medium-Density Fibreboard (MDF) to minimize thermal losses. To maintain the specified channel depth, the sidewalls (spacers) were fitted with hardwood to match the selected spacing between the heated and opposite plates. The entire test rig was mounted on a pivoting frame, allowing the angle of inclination (θ) of the channel to be adjustable. For this series of experiments, the channel was tested at three specific inclination angles: 30°, 45°, and 60° from the vertical axis. These adjustments enabled analysis to investigate the effect of the three variables (heat variations, channel aspect ratios and channel angle adjustments) on the thermal and the hydraulic performance of the system. To obtain temperature readings, Type T (copper-constantan) thermocouples with a diameter of 0.2 mm were carefully inserted at different locations within the test rig, as shown in **Figure** 1. These locations included inlet and outlet airflow points, the heated wall, the opposite wall and the ambient temperature. To prevent undesirable readings of air temperature within the channel, each thermocouple in the airstream was housed in a lightweight radiation shield to minimize the radiation effect from both plates. These shields were made from thin plastic drinking straws, about 2 cm in length, and were silvered to reflect radiant heat. To measure the airflow velocity entering the channel during experiment, a hot bead anemometer (Airflow TA-5) was employed. The device is provided by an analogue DC voltage output, which was employed and attached to a data acquisition system. According to device manual, the anemometer had been calibrated at BSRIA Instrument Solutions, achieving an operational velocity range of 0.01 to 1.25 m/s with a measurement tolerance of ±(2% of reading or 0.01 m/s), ensuring high precision in airflow monitoring. To ensure accurate results, all thermocouples were calibrated at the freezing and boiling points prior to the commencements of the experiment. The standard deviation of the calibration results at a 95% confidence level generally varied by ±0.5°C, while airflow temperature measurements exhibited fluctuations of up to ±0.8°C.

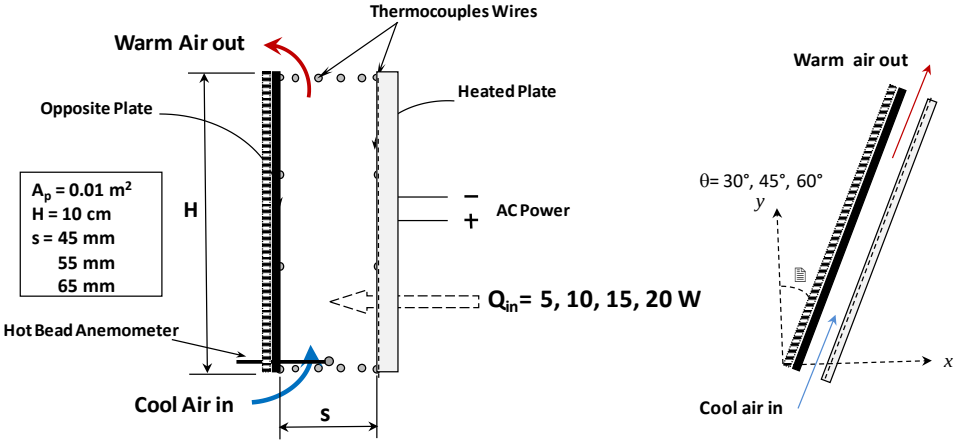

Figure 1: Experimental Apparatus.

The hot plate had a standard deviation of ±1.2°C, whereas its counterpart showed a standard deviation of ±0.9°C. Propagation rules were used to calculate the uncertainty values. Each test run commenced from a cold state (ambient temperature) and was heated for a minimum of 2.5 hours to allow the system to reach a steady state. After each run, the system was allowed to cool overnight to ensure that the next run would begin at ambient temperature. A hot bead anemometer probe was placed centrally at the bottom of the channel (assuming a flat

velocity profile at the entrance), and readings taken every 5 minutes throughout the experiment. The final data in this study were collected and analyzed under steady-state conditions for 36 runs (Three sizes of channel depth, three different inclination angles and four values of heat inputs). These measurements were taken under steady-state conditions, and all subsequent calculations and analyses will be based on this data.

3. Data Analysis and Reduction:

As stated in the previous sections, the airflow induced by bouncy force due to natural convection heat transfer is the main point under study in the present work. The following data analysis is conducted only for steady state conditions. The first primary assessment of the airflow is to look at the variation of the mass flow against three variables - heat input (Q_{in}), aspect ratio (s/H) and inclination angle with respect to vertical position (θ°). The mass flow rate was calculated based on the channel entrance condition applying the following formula [31]:

$$\dot{m} = \rho_i \, A_C \, \bar{u}_i \qquad (2)$$

According to **Table 1**, mass flow rate ($\dot{m}$) increases steadily as the rate of heat input (Q_{in}) and channel depth (s) increases, but decreases as an inclination angle (θ) increases. In other words, as the channel approaches the vertical position ($\theta \approx 0^{\circ}$), mass flow rate increases for the same values of Q_{in} and s/H, probably due to the reduction of surface friction and an increase in the bouncy force. Higher values of mass flow rate is obtained by [29] at $\theta \approx 0^{\circ}$ - vertical position- for the same values of Q_{in} and s/H.

Table 1: Variations of Mass flow Rate at Different Inclination Angles.

Table 1a: Mass Flow (kg/s) - at 30°

	5W	10W	15W	20W
s/H = 0.45 - 45mm channel depth	5.3×10^{-4}	6.9×10^{-4}	8.5×10^{-4}	1.0×10^{-3}
s/H = 0.55 - 55mm channel depth	6.2×10^{-4}	7.8×10^{-4}	9.8×10^{-4}	1.0×10^{-3}
s/H = 0.65 - 65mm channel depth	7.2×10^{-4}	9.1×10^{-4}	1.1×10^{-4}	1.0×10^{-3}

Table 1b: Mass Flow (kg/s) - at 45°

	5W	10W	15W	20W
s/H = 0.45 - 45mm channel depth	$4.8\ 10^{-4}$	5.9×10^{-4}	6.9×10^{-4}	$8. \times 10^{-4}$
s/H = 0.55 - 55mm channel depth	5.2×10^{-4}	6.5×10^{-4}	7.8×10^{-4}	$9. \times 10^{-4}$
s/H = 0.65 - 65mm channel depth	5.8×10^{-4}	7.2×10^{-4}	8.5×10^{-4}	$1. \times 10^{-3}$

Table 1c: Mass Flow (kg/s) - at 60°

	5W	10W	15W	20W
s/H = 0.45 - 45mm channel depth	2.5×10^{-4}	3.9×10^{-4}	5.2×10^{-4}	6.7×10^{-4}
s/H = 0.55 - 55mm channel depth	3.1×10^{-4}	4.6×10^{-4}	5.8×10^{-4}	7.2×10^{-4}
s/H = 0.65 - 65mm channel depth	3.5×10^{-4}	5.1×10^{-4}	6.4×10^{-4}	7.7×10^{-4}

The second primary assessment of the airflow is to look at the calculated average heat transfer coefficient ($\bar{h}$) which is always lower in natural convection than in forced convection due to the thickness of the boundary layer caused by lower fluid velocity. It also relies on the rate of heat transfer between the heated plate and the airflow. The total energy added to the system by the expression of the bulk temperature differences leads to calculating the heat transfer coefficient as follows [32]:

$$Q_c = \dot{m} \, c_p \, (T_o - T_i) \qquad (3)$$

Thus:

$$\bar{h} = \frac{Q_c}{A_p \left(T_p - T_m\right)} \qquad (4)$$

According to **Table 2**, the calculated-average heat transfer coefficient ($\bar{h}$) increases steadily as the heat input (Q_{in}) increases, but decreases as the channel depth (s) and inclination angle (θ) increase. Meaning that, heat transfer coefficient would become higher as $\theta \approx {}^{\circ}0$ - vertical position- for the same values of Q_{in} and s/H [27, 29]

Table 2: Variations of Calculated Heat Transfer Coefficient at Different Inclination Angles

Table 2a: Average Heat Transfer Coefficient (W/m^{2}K) - at 30°

	5W	10W	15W	20W
s/H = 0.45 - 45mm channel depth	7.51	10.36	14.19	17.93
s/H = 0.55 - 55mm channel depth	6.54	9.43	13.09	16.98
s/H = 0.65 - 65mm channel depth	5.33	8.69	12.20	15.95

Table 2b: Average Heat Transfer Coefficient (W/m^{2}K) - at 45°

	5W	10W	15W	20W
s/H = 0.45 - 45mm channel depth	5.07	7.52	10.88	14.74
s/H = 0.55 - 55mm channel depth	4.55	6.89	10.26	13.75
s/H = 0.65 - 65mm channel depth	4.13	6.05	9.48	12.79

Table 2c: Average Heat Transfer Coefficient (W/m^{2}K) - at 60°

	5W	10W	15W	20W
s/H = 0.45 - 45mm channel depth	2.55	5.94	8.78	11.54
s/H = 0.55 - 55mm channel depth	1.94	5.30	8.22	10.93
s/H = 0.65 - 65mm channel depth	1.38	4.66	7.68	10.40

4. Dimensionless Correlations:

Another scope of the current project was to calculate an overall Nusselt number based on "s" and "H", Reynolds number and modified Rayleigh number and find correlations between them. Three independent variables are addressed in the current project (Q_{in}, s/H and θ). In addition, in order to complete the analysis and clarify the whole picture of the airflow performance due to natural convection in the inclined channel under the UHF heating mode, dimensionless correlations were developed between dimensionless groups and derived here. Correlations were derived by applying a multiple linear regression technique or least-square method. This would allow the results to be extended more easily to correlate dimensionless equations and compare them with results from previous studies found in the literature. Overall Nu(s) and Nu(H) are defined as the dimensionless heat transfer coefficient which are both based on the calculated heat transfer coefficient ($\bar{h}$) and the characterized length (s or H). This can be obtained as follows [32]:

$$\mathrm{Nu(s)} = \frac{\bar{h}\, s}{k_m} \qquad (5)$$

$$\mathrm{Nu(H)} = \frac{\bar{h}\, H}{k_m} \qquad (6)$$

In addition, the Reynolds number, Re(s), is typically utilized in forced convection flow applications, but in this case, it is employed here to describe the velocity or the flow rate of the air inside the channel, since there is no other dimensionless number playing the role [14, 18, 19, 29, 30]. Although the Reynolds number is typically based on the hydraulic diameter, Reynolds number in the current project is based on the channel depth (s) because the channel depth here is one of the variables under investigation. This is determined as follows [31]:

$$\mathrm{Re(s)} = \frac{\bar{u}_i\, s}{\nu_m} \qquad (7)$$

The whole calculations technique has been employed by previous researchers, such as [7-22]. To establish correlations with other dimensionless groups, the modified Rayleigh number, Ra^*, is used for the Uniform Heat Flux problem, where temperatures of the surfaces and the airflow are unknown. This can be regarded as a dimensionless expression of heat input and takes the form of Equation 1**.** To progress the derivation of the above-mentioned correlations, a basic mathematical form was initially suggested as follows:

$$y = \boldsymbol{a}\, x^{\boldsymbol{b}} \qquad (8)$$

Where ***a*** and ***b*** are constants.
a is denoted as the coefficient or scaling factor.
b is denoted as the slop/index, curve shape controller.

The logarithm of both sides of Equation 8 leads to:
log Y = log(a) + b.log (x)

Proprietary software was used to derive the regression coefficients ***a*** and ***b.*** In this type of analysis, it is usual to use dimensionless numbers, to avoid problems of dimensional consistency. Note that the derived correlations are subject to the limits of the data, as follows:

$$45\text{mm} \leq s \leq 65\text{mm}$$
$$0.45 \leq s/H \leq 0.65$$
$$30^{\circ} \leq \theta \leq 60^{\circ}$$
$$5\text{W} \leq Q_{in} \leq 20\text{W}$$
$$4.74 \times 10^{6} \leq Ra^{*} \leq 1.49 \times 10^{7}$$

4.1 Two Independent Variables Correlations (Ra^{*} and s/H):

The initial derivation of the empirical correlations was considered for the two variables setting (Q_{in} and s/H) for every individual inclination angle "θ". In accordance with Equation 8, the general mathematical form of empirical correlations become:

$$\text{Nu}(s) = a\,(\text{Ra}^{*}\ s/\text{H})^{b} \quad (9)$$
$$\text{Nu}(\text{H}) = a\,(\text{Ra}^{*}\ s/\text{H})^{b} \quad (10)$$
$$\text{Re}(s) = a\,(\text{Ra}^{*}\ s/\text{H})^{b} \quad (11)$$

Where "***a***" and "***b***" are the empirical constants determined by the linear regression analysis achieved from Sigmaplot software outcomes.

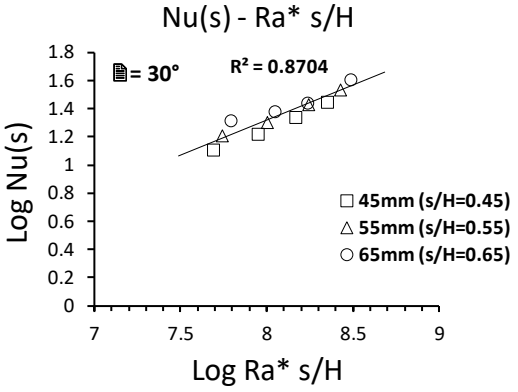

(2a): Nu(s) -- Ra^{*} s/H (30˚)

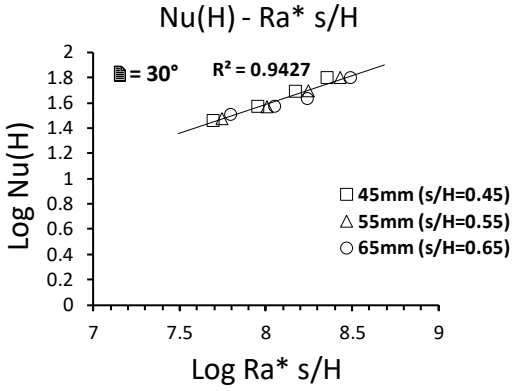

(3b): Nu(H) -- Ra^{*} s/H (30˚)

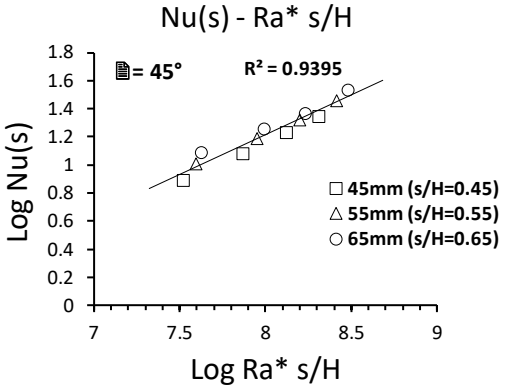

(2b): Nu(s) -- Ra^{*} s/H (45˚)

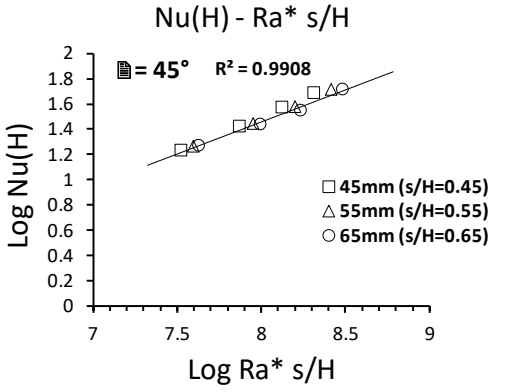

(3b): Nu(H) -- Ra^{*} s/H (45˚)

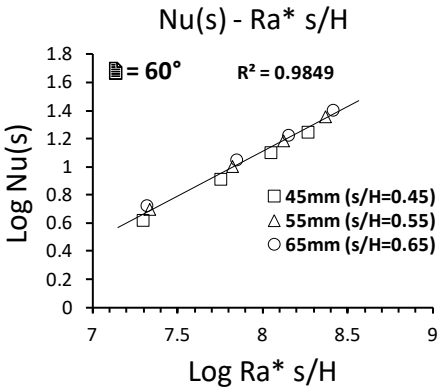

(2c): Nu(s) -- Ra^* s/H (60°)

Figure 2: Variations of Nu(s) against Ra^* s/H

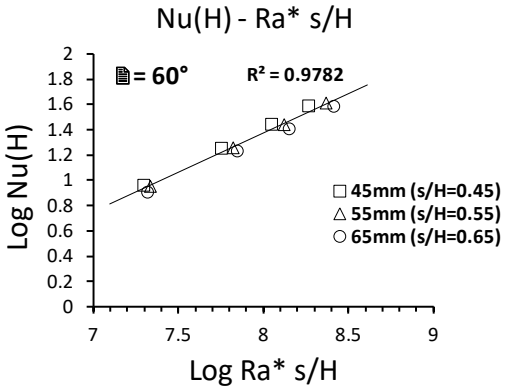

(3c): Nu(H) -- Ra^* s/H (60°)

Figure 3: Variations of Nu(H) against Ra^* s/H

Figures " **2a**, **2b** and **2c''** illustrate the variations of Nu(s) against Ra^*(s/H). All figures show that Nu(s) increases linearly as Ra^*(s/H) increases. Equations 12, 13 and 14 show the outcome correlations and attached with statistical regression data:

$$Nu(s) = 0.0023(Ra^* \ s/H)^{0.496} \quad (12)$$

*Statistical results show that: R^2= 0.87; mean percentage error of the data from the calculated regression line: 5.4%; **a** constant = 0.0023: standard error: 0.49 (t-ratio: -5.4); index for Ra^* s/H (**b** constant) =0.496: standard error: 0.0605 (t-ratio: 8.193).*

$$Nu(s) = 0.0005 \ (Ra^* \ s/H)^{0.566} \quad (13)$$

*Statistical results show that: R^2= 0.94; mean percentage error of the data from the calculated regression line: 4.9%; **a** constant = 0.0005: standard error: 0.3651 (t-ratio: -9.074); index for Ra^* s/H (**b** constant) = 0.566: standard error: 0.0454 (t-ratio: 12.458).*

$$Nu(s) = 0.0001 \ (Ra^* \ s/H)^{0.638} \quad (14)$$

*Statistical results show that: R^2= 0.99; mean percentage error of the data from the calculated regression line: 3.3%; **a** constant = 0.0001: standard error: 0.1978 (t-ratio: -20.186); index for Ra^* s/H (**b** constant) = 0.638: standard error: 0.025 (t-ratio: 25.497).*

According to Equations 12 to 14, the constant ***b*** (index or slop) increases as the inclination angle (θ) increases, whereas the constant ***a*** decreases as the inclination angle (θ) increases for the same values of Ra^* and s/H. Correlation coefficients were 87% , 94% and 99% in Equations 12, 13 and 14 respectively. It means that 87%, 94% and 99% of the variance in Nu(s) is explained by Ra^* s/H in Equations 12, 13 and 14 respectively.

Moreover, **Figures** "**3a, 3b** and **3c''** illustrate the variations of Nu(H) against Ra^*(s/H). All figures show that Nu(H) increases linearly as Ra^*(s/H) increases and their correlations outcome along with statistical data are:

$$Nu(H) = 0.0089(Ra^* \ s/H)^{0.455} \quad (15)$$

*Statistical results show that: R^2= 0.94; mean percentage error of the data from the calculated regression line: 3.1%; **a** constant = 0.0089: standard error: 0.2869 (t-ratio: -7.137); index for Ra^* s/H (**b** constant) =0.455: standard error: 0.0354 (t-ratio: 12.828).*

$$Nu(H) = 0.0017(Ra^* \ s/H)^{0.531} \quad (16)$$

*Statistical results show that: R^2= 0.97; mean percentage error of the data from the calculated regression line: 2.8%; **a** constant = 0.0017: standard error: 0.2049 (t-ratio: -13.194); index for Ra^* s/H (**b** constant) =0.531: standard error: 0.0261 (t-ratio: 20.3577).*

$$Nu(H) = 0.0003(Ra^* \ s/H)^{0.622} \quad (17)$$

*Statistical results show that: R^2= 0.87; mean percentage error of the data from the calculated regression line: 3.9%; **a** constant = 0.0003: standard error: 0.2319 (t-ratio: -15.515); index for Ra^* s/H (**b** constant) =0.622: standard error: 0.0293 (t-ratio: 21.1841).*

According to Equations 15 to 17, the constant ***b*** (index or slop) also increases as the inclination angle (θ) increases, whereas the constant ***a*** also decreases as the inclination angle (θ) increases for the same values of Ra^* and s/H. Correlation coefficients were 94% , 99% and 98% in Equations 15, 16 and 17 respectively. It means that 94% , 99% and 98% of the variance in Nu(H) is explained by Ra^* s/H in Equations 12, 13 and 14 respectively. The index/slop in most derived correlations in natural convection was found to be between 0.2 and 0.25 [20-23] particularly those under the UWT heating mode. Whereas, the index/slop here is more than a double (over 0.5) [27, 29]. This can be attributed to the fact that the Ra^* is based on H and Q_c, where Ra in the UWT is based on "s" and the temperature differences which is usually lower than Ra^*.

Similarly, in order to find relationship between Re(s) and $Ra^*(s/H)$ for every single channel inclination angle "θ" following the same technique, **Figures** "**4a, 4b** and **4c**" show the variations of Re(s) against $Ra^*(s/H)$. It is clearly observed that as Re(s) increases Ra^*s/H increases for all inclination angles "θ" and their correlations outcomes along with statistical data are written bellow:

$$\mathrm{Re(s)} = 0.7983(\mathrm{Ra^*\ s/H})^{0.341} \quad (18)$$

*Statistical results show that: R^2= 0.97; mean percentage error of the data from the calculated regression line: 1.6%; **a** constant = 0.7983: standard error: 0.1423 (t-ratio: -0.6873); index for Ra^* s/H (**b** constant) =0.341: standard error: 0.0175 (t-ratio: 19.417).*

$$\mathrm{Re(s)} = 1.2588(\mathrm{Ra^*\ s/H})^{0.338} \quad (19)$$

*Statistical results show that: R^2= 0.98; mean percentage error of the data from the calculated regression line: 2.7%; **a** constant = 1.2588: standard error: 0.1389 (t-ratio: 0.7159); index for Ra^* s/H (**b** constant) =0.338: standard error: 0.0172 (t-ratio: 17.789).*

$$\mathrm{Re(s)} = 0.5629(\mathrm{Ra^*\ s/H})^{0.330} \quad (20)$$

*Statistical results show that: R^2= 0.99; mean percentage error of the data from the calculated regression line: 1.3%; **a** constant = 0.5629: standard error: 0.0767 (t-ratio: -3.2529); index for Ra^* s/H (**b** constant) =0.330: standard error: 0.0097 (t-ratio: 34.854).*

According to Equations 18 to 20, the constant ***b*** (index or slop) is about 0.33 for all cases indicating that Re(s) α $(Ra^*s/H)^{\approx 0.33}$ agreed with [17] who found that mass flow rate is proportional to $Ra^{*1/3}$. Whereas the constant ***a*** does not show a clear trend or presentation for all cases. The potential cause may attribute to experimental error (thermocouple misreading) or change in flow pattern. Correlation coefficients were 97% , 98% and 99% in Equations 18, 19 and 20 respectively. It means that 97%, 98% and 99% of the variance in Re(s) is explained by Ra^* s/H in Equations 18, 19 and 20 respectively.

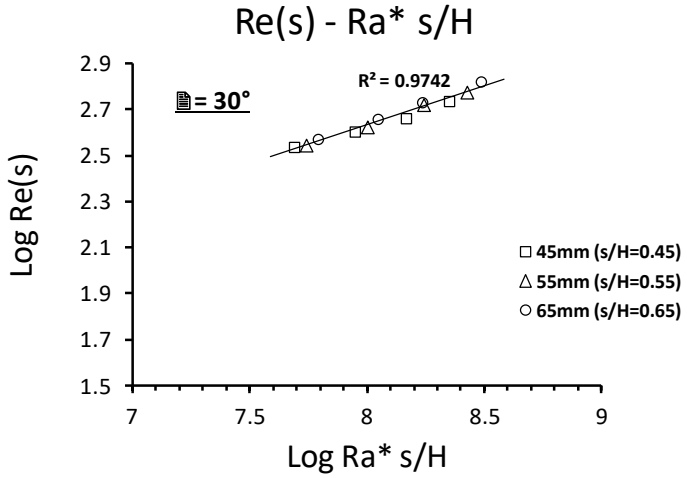

(4a): Re(s) -- Ra^* s/H at (30°)

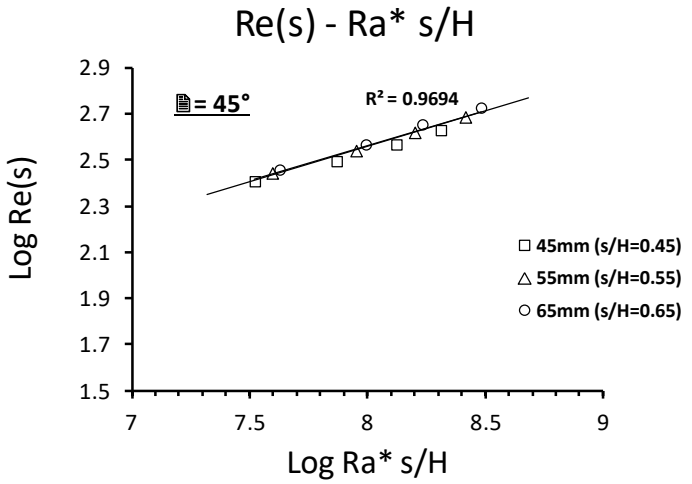

(4b): Re(s) -- Ra* s/H at (45°)

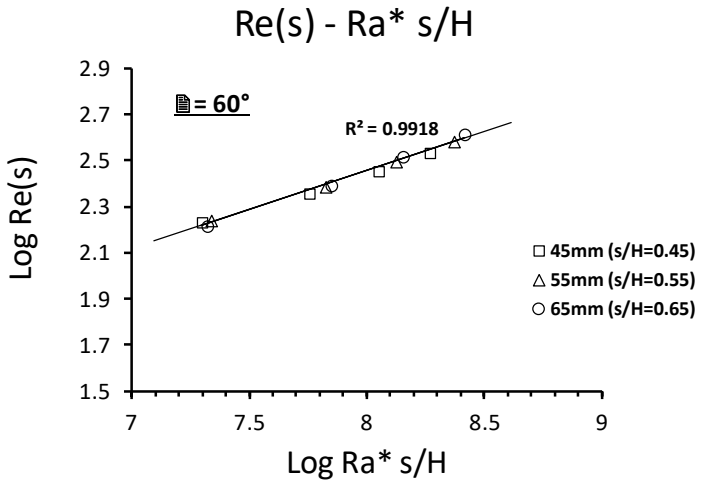

(4c): Re(s) -- Ra* s/H at (60°)

Figure 4: Variations of Re(s) against Ra* s/H

4.2 Three Independent Variables Correlations (Ra*, s/H and θ):

To sum up and narrowing all data analysis and present them in one single correlation for all cases (all heat inputs, all aspect ratios and all inclination angles). The following empirical correlations expressing heat transfer rate and flow rate in the forms of Nu(s) and Nu(H) and Re(s) against all variables Ra*, s/H and θ. According to Equation 8, the general mathematical form will take the following form:

$$\mathrm{Nu(s)} = a(\mathrm{Ra}^* \ \mathrm{s/H}\cos\theta)^b \quad (21)$$

$$\mathrm{Nu(H)} = a(\mathrm{Ra}^* \ \mathrm{s/H}\cos\theta)^b \quad (22)$$

$$\mathrm{Re(s)} = a(\mathrm{Ra}^* \ \mathrm{s/H}\cos\theta)^b \quad (23)$$

Where ***a*** and ***b*** are empirical constants whose values are also determined throughout the least square method and the regression analysis using SigmaPlot software.

As a result, **Figure 5** and **6** show Nu(s) and Nu(H) being correlated against Ra*s/H cosθ which give very good presentation of linear pattern with R^2= 0.95. Equation 24 and 25 show empirical equations for Nu(s) and Nu(H) along with their detailed statistical parameters results produced by SigmaPlot software give the following:

$$Nu(s) = 0.0002(Ra^{*}\ s/H\cos\theta)^{0.62} \quad (24)$$

*Statistical results show that: R^2= 0.95; mean percentage error of the data from the calculated regression line: 5.3%; **a** constant = 0.0002: standard error: 0.1886 (t-ratio: -19.313); index for Ra^{*} s/H cosθ (**b** constant) =0.62: standard error: 0.0241 (t-ratio: 25.778).*

$$Nu(H) = 0.0006(Ra^{*}\ s/H\cos\theta)^{0.599} \quad (25)$$

*Statistical results show that: R^2= 0.96; mean percentage error of the data from the calculated regression line: 4.8%; **a** constant = 0.0006: standard error: 0.1701 (t-ratio: -18.902); index for Ra^{*} s/H cosθ (**b** constant) =0.599: standard error: 0.0216 (t-ratio: 27.628).*

Based on Equation 24 and 25, the constant ***b*** (index or slop) was around more 0.6 (more a double of 0.25, but close to 0.55 [29]) and the R^2 = 0.95 and 0.96 in both equations. It means that 95% and 96% of the variance in Nu(s) and Nu(H) is explained by Ra^{*} s/H cosθ in Equations 24 and 25 respectively.

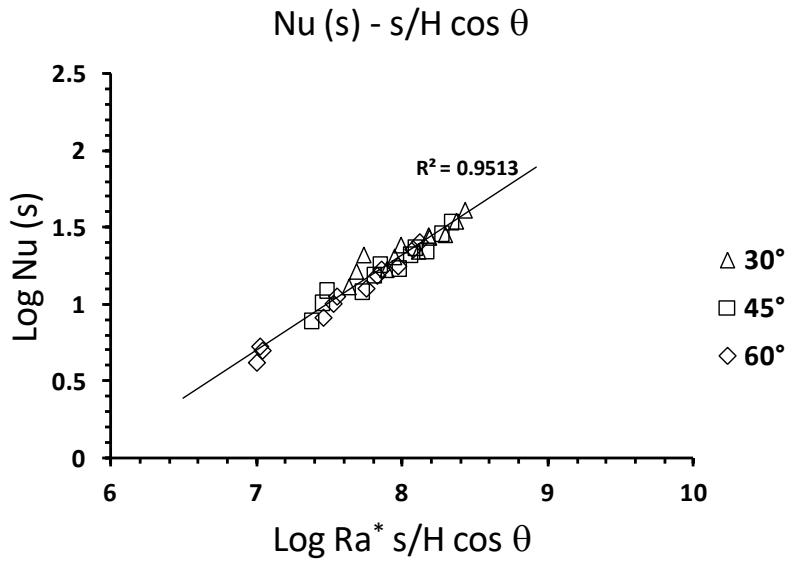

Figure 5: Variations of Nu(s) against Ra^{*} s/H cosθ

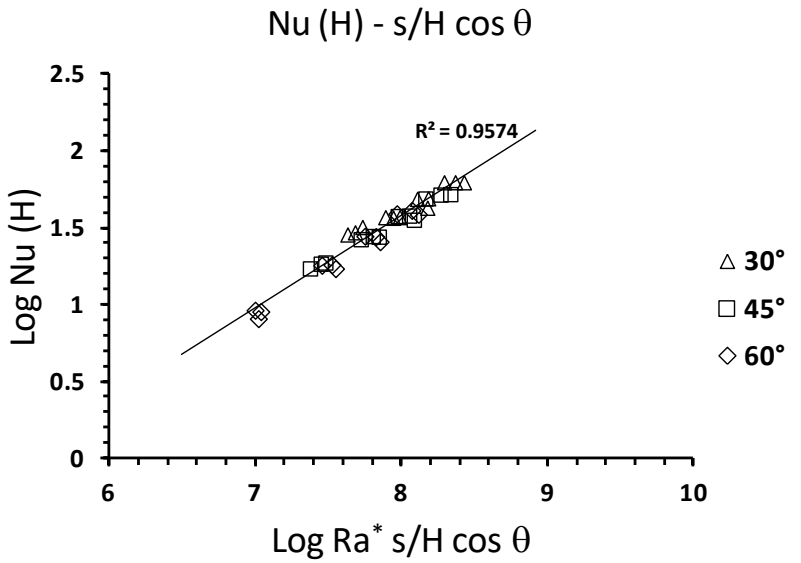

Figure 6: Variations of Nu(H) against Ra^{*} s/H cosθ

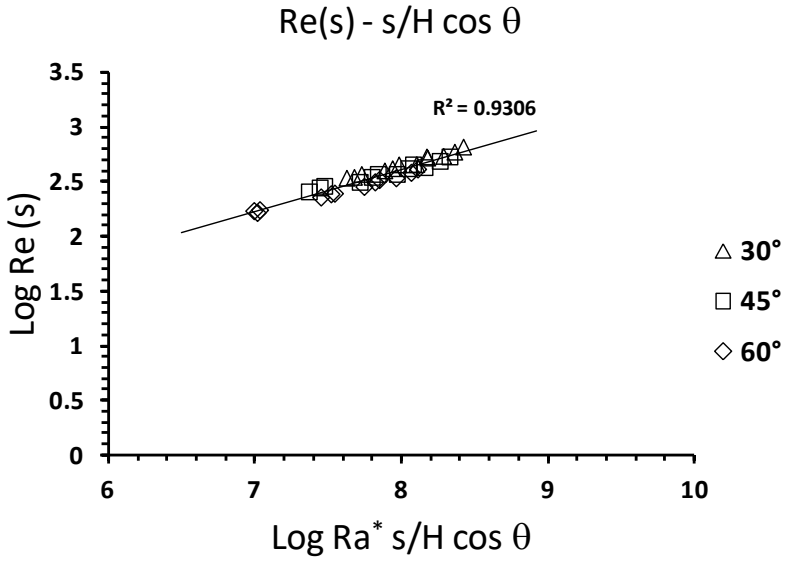

Figure 7: Variations of Re(s) against Ra^* s/H cosθ

In addition, **Figure 7** shows Re(s) being correlated against Ra^*s/H cosθ that gives very good presentation of linear pattern with R^2= 0.93. Equation 26 shows empirical equation for Re(s) along with its detailed statistical parameters results produced by SigmaPlot software that gives the following correlation:

$$Re(s)= 0.355(Ra^* \ s/H \cos\theta)^{0.383} \quad (26)$$

*Statistical results show that: R^2= 0.93; mean percentage error of the data from the calculated regression line: 3.9%; **a** constant = 0.355: standard error: 0.1406 (t-ratio: -3.1964); index for Ra^* s/H cosθ (**b** constant) =0.383: standard error: 0.0179 (t-ratio: 21.356).*

Based on Equation 26, the constant ***b*** (index or slop) was around more 0.38 (more 0.33 or 1/3) and the R^2 = 0.93. It means that 93% of the variance in Re(s) is explained by Ra^*s/H cosθ in Equations 26.

5. Discussion:

In the current work, airflow induced by bouncy force due to natural convection heat transfer was studied on an inclined closed-sided channel. An experimental investigation was carried out at three different inclination angles (30°, 45° and 60°- with respect to vertical position) under different UHF heating modes (5 W, 10 W, 15 W and 20 W) and different aspect ratios (s/H = 0.45, 0.55 and 0.65). The size of the channel was 0.1 m by 0.1 m heated uniformly from one side.

Although there was not enough data in the literature concerning UHF applications, compression of the current results with available data will be presented in this section. Calculated mass flow rate and calculated heat transfer coefficient were both presented in Table 1 and **Table** 2 respectively, for all cases. It was found that mass flow rate ($\dot{m}$) increases steadily as the heat input (Q_{in}), channel depth (s) increase and decreases as an inclination angle (θ) increases. In other words, as the channel approaches the vertical position ($\theta \approx {}^{\circ}0$), the mass flow rate increases for the same values of Q_{in} and s/H, probably due to the reduction of surface friction and an increase in the bouncy force [29]. The backflow and pockets of recirculation flow may occur and exists in such applications [20], particularly near the exit and adjacent to the opposite wall. Therefore, a simple smoke test was applied, but no visual sing of backflow or recirculation pockets was observed.

Table 2 showed the calculated-average heat transfer coefficient ($\overline{h}$). It was found that $\overline{h}$ increases steadily as the heat input (Q_{in}) increases, but decreases as the channel depth (s) and inclination angle (θ) increase. Meaning that, heat transfer coefficient would become higher as $\theta \approx {}^{\circ}0$ - vertical position - for the same values of Q_{in} and s/H, agreed with [27, 29].

Previous published empirical correlations regarding airflow and heat transfer under UHF heating mode are very few encountered in the literature. The only early correlations that are comparable to the current results are [27] and [28]. The former [27] studied airflow along an inclined surface (7.32 m high by 1.83 m wide) at angles from 30° to 80° and derived the following correlations for laminar and turbulent flow:

$$\text{Laminer Flow:} \quad Nu= 0.55\ (Ra^*)^{0.2} \quad (27)$$

$$\text{Turbulent Flow: } Nu = 0.17\,(Ra^{*})^{0.25} \quad (28)$$

Although their work was conducted on an inclined surface, its outcome correlations did not include the inclination parameter (cos2) in the formula. The latter [28] performed an analytical investigation on airflow between two vertical plates under the UWT and UHF. For the UHF case, they derived the following correlation:

$$Nu(s) = 0.204(Ra^{*}\ s/H)^{0.5} \quad (29)$$

However, on the similar current test-rig, natural convection was studied on airflow along a vertical channel ($2\approx0^{\circ}$) and derived the following correlations in heat transfer and mass flow rate [29]:

$$Nu(s) = 0.0008\,(Ra^{*}\ s/H)^{0.563} \quad (30)$$

$$Nu(H) = 0.0018\,(Ra^{*}\ s/H)^{0.551} \quad (31)$$

$$Re(s) = 0.7602\,(Ra^{*}\ s/H)^{0.357} \quad (32)$$

Accordingly, the proceeding discussion will consider Equations 27, 28, 29, 30, 31 and 32 and compare them with current results (Equation 24, 25 and 26). **Figures** 8a and 8b show the current result of Equations 24 and 25 being compared with the results of Equations 27, 28, 29, 30 and 31. Although the current result demonstrates a very good presentation, discrepancies between the current results and [27, 28] results are observed. This can be attributed to the following potential causes. The results of [27] were derived from a long tilted single surface and did not consider the inclination angle in equations 27 and 28. In addition, the range of heat transfer that was worked on [27] may be different from the current study.

Although the results from [28] are almost parallel to the current results, the lack of the accuracy of the analytical solution to derive Equation 29 may be the main cause of disagreements. In addition, the results of [28] were for vertical parallel plates ($\theta=0^{\circ}$) and not for a tilted channel. However, results presented by [29] show a very good agreement with current results with little scatter for Nu(s) and Nu(H) equations despite the equation of [29] was set for vertical position ($\theta\approx0^{\circ}$, with respect to vertical position) which has no effect as cos0=1

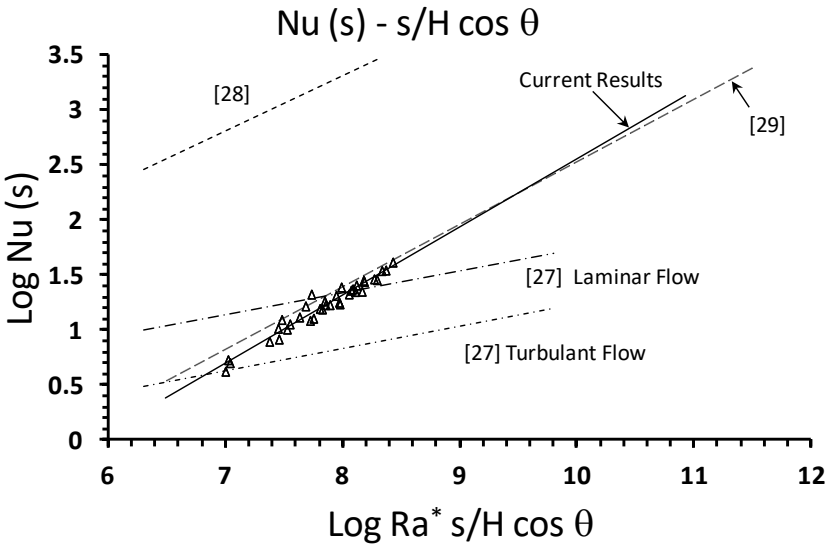

(8a): Nusselt Based on Channel Depth - Nu(s)

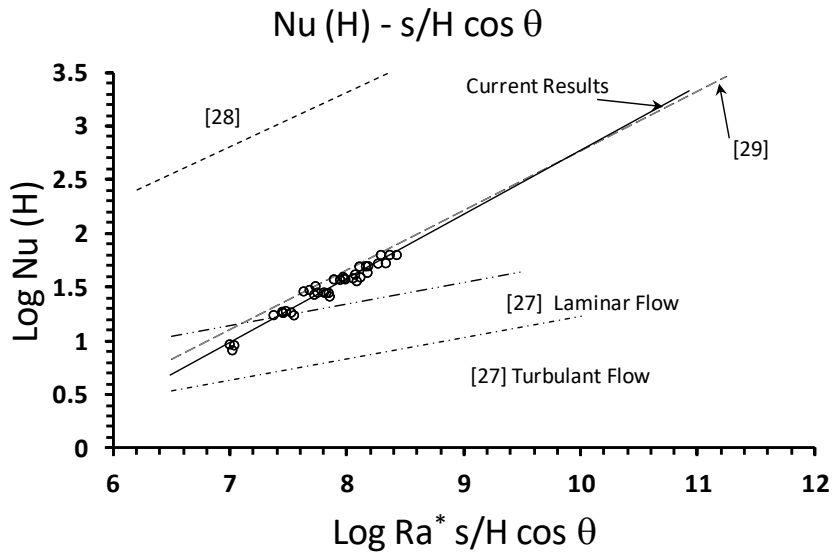

(8b): Nusselt Based on Heights - Nu(H)

Figure 8: Nusselt Numbers Compressions

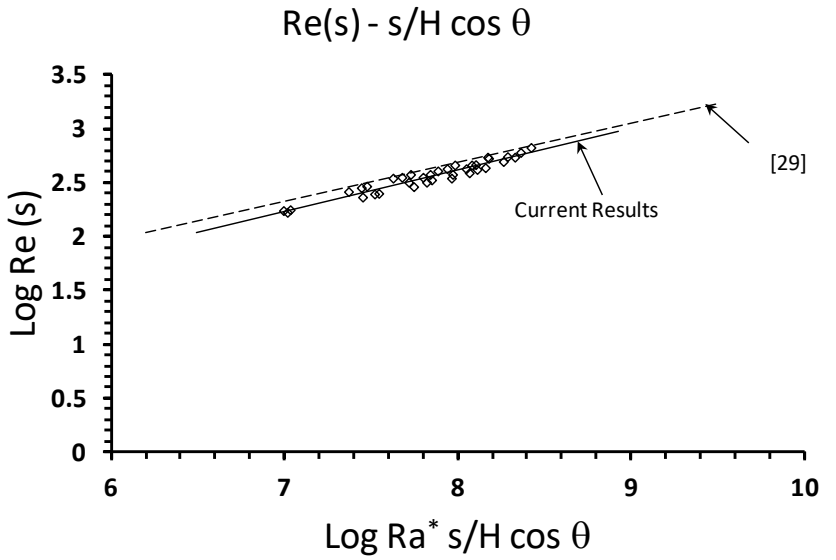

Figure 9: Reynolds Numbers Compressions

However, **Figure** 9 shows the compression of the current results (Equation 26) and the results of [29] (Equation 32). It clear that both results present shows very good agreement with little deviations despite the differences in inclination position.

Final consideration to look for a relationship between Nu and Re(s). in forced convection, determination of the heat transfer coefficient for a fully developed turbulent flow in smooth tube under the UHF mode based on bulk temperature differences, as done in Equations 3 and 4, Reference [33] presented a traditional empirical equation and takes the following form:

$$Nu = 0.023\, Re^{0.8}\, Pr^{n} \quad (33)$$

Matching the general mathematical form:

$$Nu = a\, Re^{b}\, Pr^{0.4} \quad (34)$$

Reference [33] recommended that the exponent n = 0.4 for heating condition and n = 0.3 for the cooling condition of the fluid. Therefore, and since the current situation is for heating conditions, Equation 33 can be modified as:

$$Nu = 0.023\, Re^{0.8}\, Pr^{0.4} \tag{35}$$

The equation 35 is valid for fully developed flow in UHF smooth tube for all fluids, their Pr numbers varying from 0.6 to 100. Although the current situation is applicable to pure natural convection flow, the existence of a flow in the current duct may still be comparable to the smooth horizontal tube. Therefore, **Figure** 10 shows Nu(s)/ $Pr^{0.4}$ and Nu(H)/$Pr^{0.4}$ correlated against R(s) s/H cosθ and the two correlations are derived based on the same mathematical form of equation 34. Equations 36 and 37 are presented below along with their detailed statistical parameters results produced by SigmaPlot software:

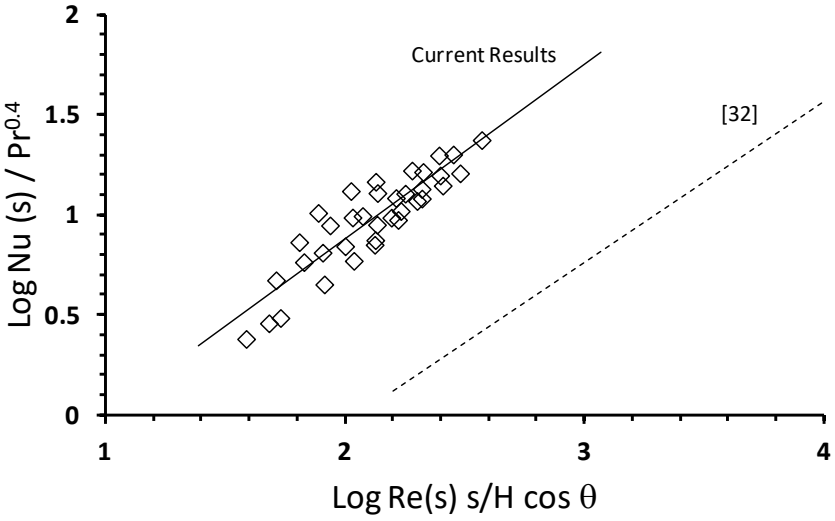

(a) Nu(s) - Re(s)

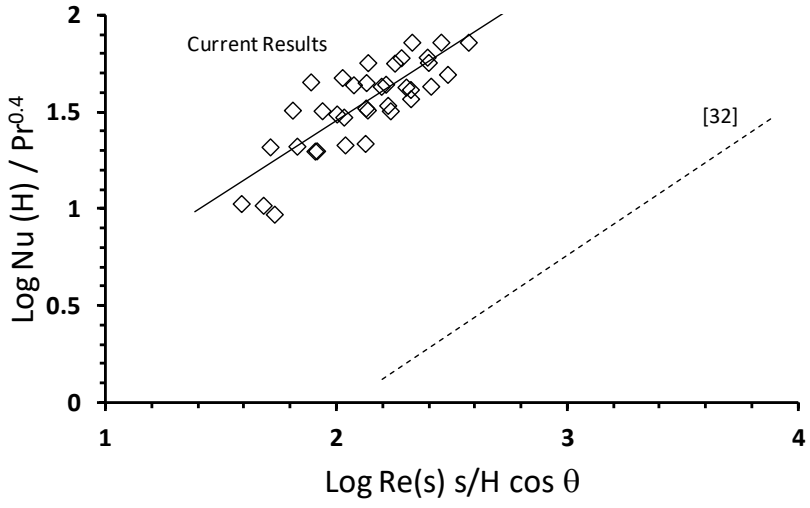

(b) Nu(H) - Re(s)

Figure 10: Nu Variations with Re(s)

$$Nu(s) = 0.1362(Re(s)\ s/H\cos\theta)^{0.871}\ Pr^{0.4} \quad (36)$$

*Statistical results show that: R^2= 0.80; mean percentage error of the data from the calculated regression line: 10.9%; **a** constant = 0.1362: standard error: 0.1594 (t-ratio: -5.432); index for Re(s) s/H cosθ (**b** constant) =0.871: standard error: 0.0748 (t-ratio: 11.6326).*

$$Nu(H) = 0.8189(Re(s)\ s/H\cos\theta)^{0.770}\ Pr^{0.4} \quad (37)$$

*Statistical results show that: R^2= 0.68; mean percentage error of the data from the calculated regression line: 13.3%; **a** constant = 0.8189: standard error: 0.1951 (t-ratio: -0.4448); index for Re(s) s/H cosθ (**b** constant) =0.770: standard error: 0.0916 (t-ratio: 8.4077).*

By comparing Equation 35 on one hand and Equation 36 and 37 on the other hand, the two sides show a modest unexpected similarity (in terms of the values of constants ***a*** and ***b*** which are all less than one (similar slop). It is not stated here that there is a strong similarity because equation 35 was obtained for a forced convection flow in a horizontal tube, whereas Equations 36 and 37 are for natural convection flow in an inclined channel. Therefore, the relationship between Nu and Re(s) requires deeper investigation in future studies because there is still qualitative agreement.

6. Conclusion:

Heat transfer by natural convection in inclined channel under a uniform heat flux is the main subject of the current work. Airflow flow and heat transfer characteristics under the variations of inclination angles, aspect ratio and heat input were experimentally investigated. Extensive analysis has led to the followings outcomes:

- Mass flow rate ($\dot{m}$) increases as the heat input (Q_{in}) and channel depth/aspect ratio (s, s/H) increase, but decreases as an inclination angle (θ) increases.
- Average heat transfer coefficient ($\overline{h}$) increases as the heat input (Q_{in}) increases, but decreases as the channel depth/aspect ratio (s, s/H) and inclination angle (θ) increase.
- The main dimensionless correlations for airflow and heat transfer rate summarized as fellow:

[1] $Nu(s) = 0.0002(Ra^*\ s/H\cos\theta)^{0.620}$

[2] $Nu(H) = 0.0006(Ra^*\ s/H\cos\theta)^{0.599}$

[3] $Re(s) = 0.3550(Ra^*\ s/H\cos\theta)^{0.383}$

Further Work:

Two important issues should be considered as an extension of this work. The classification of the flow regime for a laminar, transition and turbulent flow under the UHF heating mode should be determined and their relative correlations should be derived. It is also important to apply a visual technology to measure the airflow such as the PIV (Particle Image Velocimetry) apparatus to detect and trace, for example, backflow or a change in the flow pattern. Developing a CFD model is also crucial to reduce time and physical efforts.

Nomenclature:

a, b	Empirical constants (see Equation 8, 9, 10, 11, 21, 22, 23, 34).
A_C	Cross section area of the channel (s x w) m^2.
A_P	Hot plate Area ($0.01m^2$).
c_p	Specific heat at constant pressure (J/kg/K)
Gr(H)	Grashof number based on H ($Gr(H) = \frac{g\,\beta\,\Delta T\,H^3}{\nu^2}$).
g	Acceleration due to gravity (= 9.81 m/s^2).
$\bar{h}$	Convective heat transfer (W/m^2K).
H	Channel height = 1m.
k_m	Thermal conductivity of air (W/m.K).
$\dot{m}$	Airflow rate (kg/s).
Nu (s)	Nusselt Number based on channel depth (s).
Nu(H)	Nusselt Number based on channel height (H).
Pr	Prandtl number.
Q_c	Convective heat to airstream (W/m^2)
Q_{in}	Heat input (W/m^2).
Ra^*	Modified Rayleigh nember.
Ra(s)	Rayleigh number ($Ra(s) = g\,\beta\,\Delta T\,s^3/\nu^2\,.Pr$).

Re(s)	Reynolds number based on channel depth (s).
s	Channel depth (m).
T_i	Inlet mean temperature (°C).
T_a	Ambient Temperature (°C).
T_m	Mean temperature of air in the channel = $[(T_i+T_o)/2]$ (°C).
T_o	Outlet mean temperature (°C).
T_p	Hot plate mean temperature (°C).
$\bar{u}$	Air bulk velocity (m/s).
w	Channel width = 0.1m.
x	Independent Variable in (Equation 8)
y	Dependant Variable in (Equation 8).

Greek symbols:

β	Expansion coefficient (1/K).
θ	inclination angel (degree)
ρ_i	Density (kg/m^3).
υ_m	Kinematic viscosity (m^2/s).

References:

[1] R. Cheesewright, "Turbulent natural convection from a vertical plane surface", Journal of Heat Transfer, 1968, vol. 90, pp. 1-8.

[2] Y. Warner Charles and S. Arpaci Vedat, "An experimental investigation of turbulent natural convection in air at low pressure along a vertical heated flat plate", Int. J. Heat Mass Transfer, 1968, Vol. 11, pp. 397-406.

[3] E.M. Sparrow, and J.L. Gregg, "Similar solutions for free convection from a nonisothermal vertical plate", Transactions of the ASME, 1958, vol. 80, pp. 379-386.

[4] G.C. Vliet, and C.K. Liu, "An experimental study of turbulent natural convection boundary layers", Journal of Heat Transfer, 1969, pp. 517-531.

[5] S.W. Churchill, and H.H.S. Chu, "Correlating equations for laminar and turbulent free convection from a vertical plate", International Journal of Heat and Mass Transfer, 1975, vol. 18, pp. 1323-1329.

[6] W. Elenbaas, "Heat Dissipation of parallel plates by free convection", Physica, 1942, vol. 9. Pp. 1-24.

[7] E. M. Sparrow, and , P.A. Bahrami, "Experiments on natural convection from vertical parallel plates with either open or closed edges", Journal of Heat transfer, 1980, vol. 102, pp. 221-227.

[8] E. M., Sparrow, G. M. Chrysier and L. F. Azevedo, "Observed flow reversals and measured-predicted Nusselt Number for natural convection in a one-sided heated vertical channel", Journal of Heat Transfer, 1984, pp. 325-332.

[9] E. M. Sparrow and L. F. A. Azevedo, "Vertical-channel natural convection spanning between the full-developed limit and the single-plate boundary-layer Limit", Int. J. Heat and Mass transfer, 1985, Vol. 28, No. 10, pp. 1847-1857.

[10] B.W. Webb, and D.P. Hill, "High Rayleigh Number laminar natural convection in an asymmetrically heated vertical channel". Journal of Heat Transfer, 1989, vol. 111, pp. 649-656.

[11] W. M. Lewandowski, M. Ryms, and H. Denda, "Natural convection in symmetrically heated vertical channels", International Journal of Thermal Sciences, 2018, vol. 134, 530-540.

[12] S., Foroushani, D., Naylor, and J. L., Wright, "Heat transfer correlations for laminar free convection in vertical channels with asymmetrically heated isothermal walls", 2020, Heat Transfer Engineering, vol.41, pp. 418-432.

[13] D., Talukdar, C. G., Li, and M. Tsubokura, "Numerical investigation of laminar compressible natural convection flow in asymmetrically and isothermally heated open-ended inclined channel" International Journal of Heat and Mass Transfer, 2019, vol. 130, 83-97.

[14] A. G., Fedorov and R. ,Viskanta, "Turbulent natural convection heat transfer in an asymmetrically heated vertical parallel-plate channel", Int. J. Heat and Mass Transfer, 1997, vol. 16, No. 16, pp. 3849-3860.

[15] M.A., Habib, S.A.M Said, and A.A. Asghar, "Velocity characteristics of turbulent natural convection in symmetrically and asymmetrically heated vertical channels", Experimental Thermal and Fluid Science, 2002, vol. 26, pp. 77-87.

[16] N. A. A., Qasem, , B., Imteyaz, R., Ben-Mansour, and M. A. Habib, "Effect of radiation heat transfer on naturally driven flow through parallel-plate vertical channel", Arabian Journal for Science and Engineering, 2017, vol. 42, pp. 1817–1829.

[17] M., Sandberg, and B., Moshfegh, "Buoyancy-induced air flow in photovoltaic facades: effect of geometry of the air gap and location of solar cell modules", Building and Environment, 2002, vol. 37(3), 211-218.
[18] A., La Pica, G., Rodonò, and R., Volpes, "An experimental investigation on natural convection of air in a vertical channel, International Journal of Heat and Mass Transfer, 1993, vol. 36(3).
[19] S. A. M., Burek, and A., Habeb, "Air flow and thermal efficiency characteristics in solar chimneys and Trombe walls", Energy and Buildings, 2007, vol. 39(2), pp. 128-135.
[20] L. F. A., Azevedo and E. M., Sparrow, "Natural convection in open-ended inclined channels", Journal of Heat Transfer, 1985, vol. 107, pp. 893-901
[21] N., Onur, M., Sivrioglu, and M. K., Aktas, "An experimental study on the natural convection heat transfer between inclined plates (lower plate isothermally heated and the upper plate thermally insulated as well as unheated)", Heat and Mass transfer, 1997, vol. 32(6), pp. 471-476.
[22] N., Onur, and M. K., Aktaş, "An experimental study on the effect of opposing wall on natural convection along an inclined hot plate facing downward" International Communications in Heat and Mass Transfer, 1998, vol. 25(3).
[23] S., Baskaya, M. K., Aktas, and N., Onur, "Numerical simulation of the effects of plate separation and inclination on heat transfer in buoyancy driven open channels", Heat and Mass Transfer, 1999, vol. 35(4), 273-280.
[24] T., Khoualdi, M. S., Rouabah, M., Bouraoui, A., Abidi-Saadb, and G., Polidori, "Free convection heat transfer in an inclined channel asymmetrically heated in laminar regime", International Journal of Heat and Technology, 2018, vol. 36(3).
[25] A., Andreozzi, B., Buonomo, Y., Jaluria, and O., Manca, "Numerical investigation on natural convection in inclined channels partially filled with asymmetrically heated metal foam", Journal of Heat and Mass Transfer, 2023, vol. 145(4).
[26] E. M., Sparrow, and J. L., Gregg, "Laminar free convection from a vertical plate with uniform surface heat flux", Transactions of the ASME, 1956, vol. 78, pp. 435–440.
[27] G. C., Vliet, and D. C. Ross, "Turbulent natural convection on upward and downward facing inclined constant heat flux surfaces", Journal of Heat Transfer, 1975, pp: 549-554.
[28] A., Bar-Cohen and W. M, Rohsenow, "Thermally optimum spacing of vertical natural convection cooled, parallel plates", Journal of Heat Transfer, February, 1984, vol. 106, pp. 116-123.
[29] Habeb, A., "Airflow performance in close-sided vertical channel", Libyan Journal of Contemporary Academic Studies, 2025, vol. 1(3), pp. 280-291.
[30] A., Habeb, "Airflow and heat transfer by natural convection in small-scale vertical channel", 1st International Conference on Chemical, Petroleum, and Gas Engineering (ICCPG), 2016, Al-Mergib University, Libya.
[31] B., R., Munson, and T., H., Okiishi, W., W., Huebsch, and A., P., Rothmaayer, "Fundamentals of fluid mechanics", 2021, John Wiley & Sons, Inc.
[32] F., Incropera, D., Dewitt, T., Bergman, and A., Lavine, "Fundamentals of heat and mass transfer", 2016, John Wiley and Sons.
[33] Holman, J. P., "Heat Transfer", 2010, McGraw-Hill.